Research Article

Poly(bisphenol A-co-epichlorohydrin) and Nanodiamonds/Poly(azo-pyridine)/Polyamide/Multi-walled Carbon Nanotube-based Nanofiber Nanocomposites

Ayesha Kausar

Nanosciences and Catalysis Division, National Centre For Physics, Quaid-i-Azam University,

Pakistan

Abstract

Polyamide was grafted on multi-walled carbon nanotube (MWCNT) to produce MWCNT-PA using γ-Phenyl-ε-caprolactone via in-situ polymerization. For the preparation of nanofiber poly(azo-pyridine) (PAP) was also synthesized in this work. MWCNT-PA was then electrospun with PAP and nanodiamond (ND) to yield two types of nanofiber i.e. ND/PAP/MWCNT/PA and PAP/MWCNT/PA nanofibers. Subsequently, poly(bisphenol A-co-epichlorohydrin) (PBAE) was reinforced with electrospun nanofiber to form two types of nanocomposites, with and with out nanodiamond. Scanning and transmission electron microscopy showed that the nanofiber was evenly coated with the epoxy having spherical beads due to agglomeration of matrix at certain places. Tensile studies depicted higher tensile stress value 330.3-341.3 MPa for ND/PAP/MWCNT/PA/PBAE nanocomposite compared with PAP/MWCNT/PA/PBAE nanocomposites without nanodiamonds i.e. 288.1-299.9 MPa. Thermal stability of ND/PAP/MWCNT/PA nanofiber reinforced epoxy was significantly higher T_{10} 536-546 ℃ and T_g 301-311 ℃ relative to PAP/MWCNT/PA system. Another advantage of the inclusion of nanodiamond in nanofiber was the increased electrical conductivity of ND/PAP/MWCNT/PA/PBAE nanocomposites in the range 4.1-5.5 Scm^{-1}. Owing to outstanding properties of ND/PAP/MWCNT/PA/PBAE, imperative electronic, optical and aerospace industrial applications are expected.

*Correspondence to: Ayesha Kausar, Nanosciences and Catalysis Division, National Centre For Physics, Quaid-i-Azam University, Islamabad, Pakistan; Email: asheesgreat@yahoo.com

1. Introduction

Continuous nanofibres can be prepared from polymer solution/melt in the presence of high electric field using electrospinning [1, 2]. This process offers an uncomplicated route to fabricate polymer fibers with diameters ranging from nanometers to micrometers. The principal benefit of polymeric nanofibers has been the huge increase in the surface area to volume ratio. Recently, polymer fiber mats have been prepared using the cost effective electrospinning process. These electrospun fiber mats have been employed in water filters, textiles, sound absorbers materials, gas sensors, etc. Numerous studies have been reported addressing various aspects of electrospinning process [3-6]. Major factors affecting the electrospinning process include solution viscosity, surface tension, electric field intensity, distance, etc. The use of electrospun nanofibrous mats has also attracted a great deal of attention in biomedical applications. Through a systematic study of electrospinning parameters, nanofibers have been produced using different types of polymers [7-11]. Small diameter, large surface area, and small pore size render polymeric nanofibers commercially important materials in various industrial applications such as filtration media, catalysis, adsorption, etc. Applications of these nano-size fibers have been further widened due to higher length to diameter ratio and small mass to volume ratio. The properties of nano fibres have been exploited by researchers to determine appropriate conditions for electrospinning various polymers and biopolymers for eventual applications including multifunctional membranes, tissue engineering, drug delivery and artificial organs [12, 13]. Design of the polymeric nanofibres to convene explicit desires for functional relevance requires a thorough acquaintance of the electrospinning parameters and their effect on nanofiber diameters and morphology [14, 15]. The unique structural and topological characteristics, small size, confer on carbon nanotube (single walled carbon nanotube (SWCNT) and multi-walled carbon nanotube (MWCNT) with excellent electrical, mechanical, thermal, chemical and optical properties [16-18]. The potential of carbon nanotube is, therefore, revolutionized in the development of nanocomposites and nanodevices [19, 20]. Consequently, the nanoscale structures have been incorporated in a variety of materials at macroscopic level, by means of various techniques. In this regard, conventional polymeric fibers have been reinforced with carbon nanofiller to produce ultra-light composite material with enhanced physical properties [21].

Generally, epoxy resins has been known for their excellent adhesion, chemical and heat resistance, mechanical properties, electrical insulation, etc. [22, 23]. To expand the applications of this resin, there is need to cure it due to its brittleness causing low impact strength. In recent times, nanofiber reinforcement has been identified as a supportive technique to improve the mechanical properties of epoxy composite [24, 25]. There is an extensive employment of thermoplastics in toughening of epoxy resins and composites. In this regard, polyamide/polyimide nanofibers have been used for toughening the epoxy composite. In this endeavor, we have functionalized the MWCNT *via* Friedel-Crafts acylation of 2-(3-amino-propylamino)nicotinic acid using polyphosphoric acid and P_2O_5 as drying reagents. Afterwards, functionalized MWCNT was grafted with γ-phenyl-ε-caprolactone using stannous octoate as catalyst. The polyamide-*grafted*-nanotube (MWCNT-PA) was then electrospun with new polyazopyridine (PAP) and/or nanodiamond (ND). The electrospun ND/PAP/MWCNT/PA and PAP/MWCNT/PA nanofibers were used to reinforce the poly(bisphenol A-co-epichlorohydrin) to increase the interfacial binding with the matrix. In

this way two types of nanofibrous membranes, ND/PAP/MWCNT/PA/PBAE and PAP/MWCNT/PA/PBAE, have been prepared i.e. with and without nanodiamond. The structural features, morphology, thermal and mechanical stability of nanocomposites have been explored. The fracture surface of nanocomposites was examined by scanning electron microscopy (SEM). The electrical conductivity of the nanocomposites was also examined. An important feature of this research was the production of non-woven nanofibrous membranes. Such type of membranes with exclusive morphology, high porosity, enhanced mechanical, electrical and thermal performance permit immense potential for various applications such as nano-sensors, electronic/optical industrial applications, military body armor, aerospace etc. [26].

2. Experimental

2.1. Materials

Nanodiamond powder <10 nm particle size (≥97 %), poly(bisphenol A-co-epichlorohydrin) (PBAE; average M_w ~40,000, pellets), 1,4-phenylene diamine (≥99 %), 2,6-daminopyridine (97 %), 2-(3-amino-propylamino)nicotinic acid (99 %), γ-phenyl-ε-caprolactone (99 %), stannous octoate (95 %), polyphosphoric acid (≥83 % phosphate), phosphoric pentaoxide (P_2O_5, 99 %) and N,N-dimethylacetamide (DMAc) (99 %) were procured from Aldrich (St. Louis, Missouri, USA). MWCNT was prepared by our patented technology [27]. Ammonium thiocyanate (98 %) was provided by Fluka (Biocen GmbH, Duesseldorf, Germany).

2.2. Measurements

Infrared (IR) spectra were recorded using Fourier transform infrared (FTIR) Spectrometer, Model No. FTSW 300 MX, manufactured by BIO-RAD, California, USA (4 cm^{-1} resolution). Field Emission Scanning Electron Microscopy (FE-SEM) of freeze fractured samples was performed using JSM5910, JEOL Japan. Thermal stability was verified by METTLER TOLEDO TGA/SDTA 851 (California, USA) thermo gravimetric analyzer using 3 mg of the sample in Al_2O_3 crucible at a heating rate of 10 °C/min. The dynamic mechanical thermal analysis was performed on hybrid materials in the temperature range of 0–300 ℃ with DMTA Q800 (frequency of 5 Hz, heated at 10 ℃/min). Stress-strain response of the samples was obtained on Universal Testing Machine INSTRON 4206 (Norwood, United States) according to the ASTM 638 method. A crosshead speed of 100 mm/min was used during the test. Electrical conductivity of thin films was measured using a Keithley 614 electrometer and the four-probe method.

2.3. Synthesis of monomer

1,4-Phenylenediamine (0.2 mol), 16 mL of conc. HCl, ammonium thiocyanate (0.2 mol) and 120 mL of deaerated water were heated in a porcelain dish for 2 h. The mixture was then cool to room temperature. Later, the above mixture was evaporated to dryness for 6–7 h. 1,4-Phenylene bis(thiourea) obtained was dried at 85 ℃ (36 h). Afterwards, to the concentrated hydrochloric acid (10 mL) and distilled water (50 mL), 2,6-diaminopyridine (0.04 mol) was added and cooled to -10 ℃. 0.04 mol sodium nitrite solution (20 mL) was then added. The mixture was ultrasonicated for 1 h at -10 ℃ to evade the decay of diazonium salt.

Excess of nitrite was removed by the addition of urea (2 g) resulting in diazonium salt solution.

2.4. Synthesis of azo-polymer (PAP)

1,4-Phenylene bis(thiourea) was dissolved in 10 % sodium hydroxide and diazonium salt solution obtained was added drop wise at -10 ℃. After 3 h, the mixture was acidified with 10 % dil. HCl. The resulting precipitate was filtered and washed with hot water and 3 % HCl. The precipitate was dissolved in 3 % sodium hydroxide solution followed by re-precipitation in HCl. The polymer was dried under vacuum at 80 ℃.

2.5. Functionalization of MWCNT via Friedel-Crafts acylation

In this reaction, 2-(3-amino-propylamino)-nicotinic acid, MWCNT and polyphosphoric acid were heated at 120 ℃ for 3 h. Then phosphoric penta oxide (P_2O_5) was added and mixture was heated for further 12 h. The reaction mixture was cooled, diluted with distilled water, and filtered (Scheme 1). The functionalized MWCNT were dried at 100 ℃ for 48 h [28].

2-(3-amino-propylamino)-nicotinic acid

PPA/P_2O_5

120 ℃,12 h
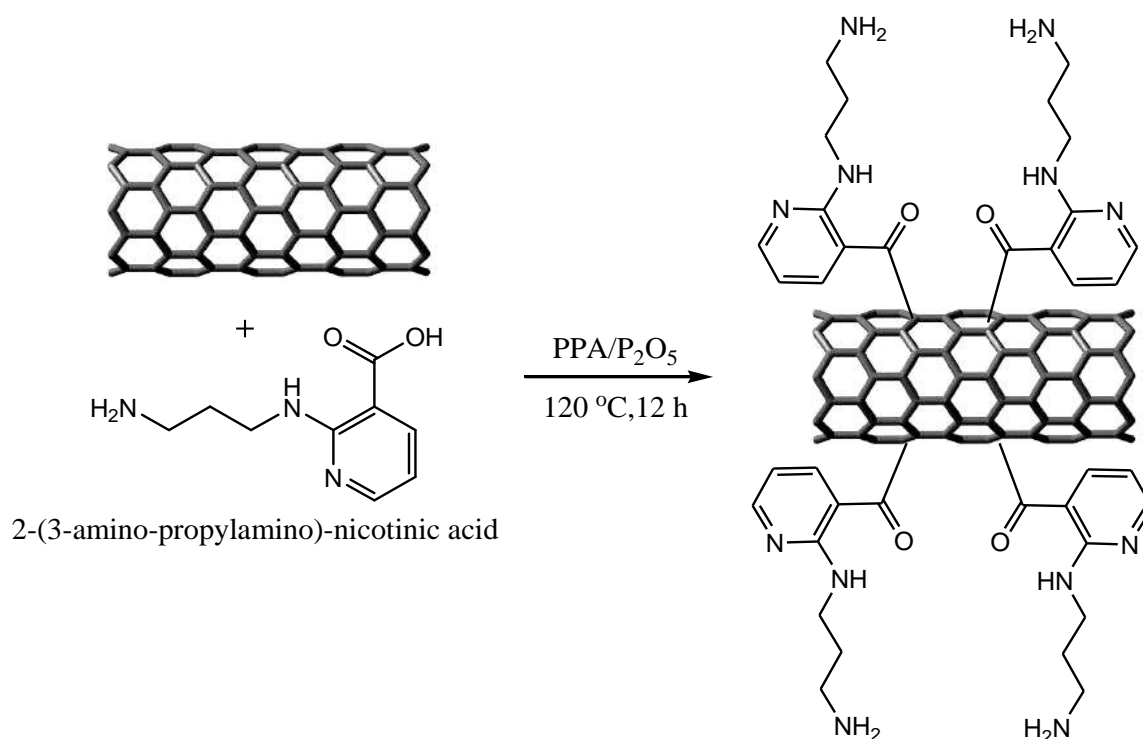
Scheme 1 Friedel-Crafts acylation of side walls of MWCNT.

2.6. Formation of MWCNT-PA via In-situ polymerization

0.1 g of above functionalized MWCNT and 20 mL γ-phenyl-ε-caprolactone were sonicated at room temperature for 3 h to obtain homogeneous dispersion of nanotube. 0.03 mL stannous octoate (Sn(Oct)$_2$) was added to the above suspension. The reaction flask was then heated to 170 ℃ for 4 h under N$_2$ (Scheme 2).
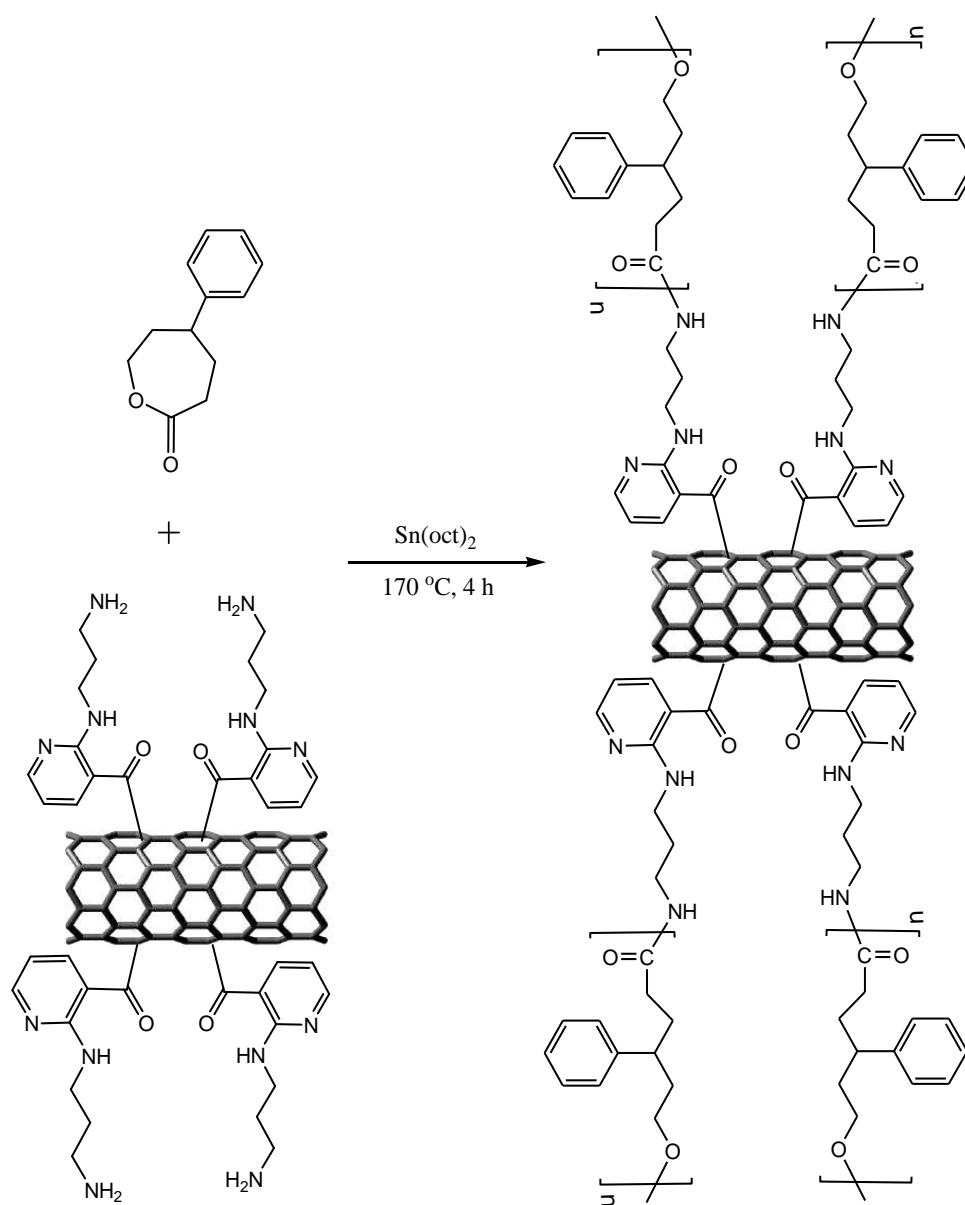
Scheme 2 Formation of MWCNT-PA *via in-situ* polymerization.

2.7. Solution preparation

The precursor solution of PAP/MWCNT/PA was synthesized by the dissolution of MWCNT-PA (5 wt. %)/PAP (25 wt. %) in DMAc. On the other hand, MWCNT-PA (5 wt. %)/PAP (25 wt. %) solution was prepared in DMAc and was diluted with 5 wt. % ND/DMAc solution for ND/PAP/MWCNT/PA. 5 wt. % ND/DMAc solution was first sonicated for 5 h prior to solution mixing to get homogeneous dispersion.

2.8. Preparation of nanofiber via electrospinning

A syringe alongwith a spinneret (diameter 0.5 mm) was used for electrospinning (25 kV; 30 ℃). The spinneret-collector distance was set to be 10 cm and feeding rate was attuned at 0.25 mL/h. ND/PAP/MWCNT/PA and PAP/MWCNT/PA nanofibers were fabricated *via* rotating disk collector (diameter 0.30 m; width 10 mm). During electrospinning, the linear speed of rotating collector was about 10 ms^{-1}. All the electrospun nanofiber was dried at 120 ℃ for 12 h.

2.9. Preparation of nanofiber reinforced films

2 g epoxy PBAE was reinforced with the required amount of as-prepared electrospun nanofiber (ND/PAP/MWCNT/PA and PAP/MWCNT/PA) and sonicated for 1 h and heated to 100 ℃. The mixture was poured into Petri dish to obtain films. The structural analysis of nanofiber and its nanocomposite is given in Fig. 1 and Table 1 [29].
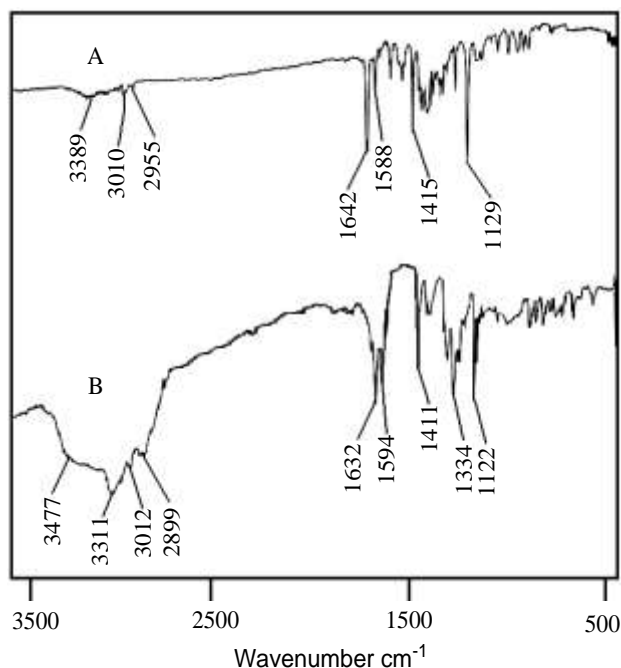

Figure 1 FTIR spectra of (A) ND/PAP/MWCNT/PA nanofiber and (B) ND/PAP/MWCNT/PA/PBAE 1.

Table 1 Spectral data of PAP, nanofiber and nanocomposite.

Compound	FTIR	
	Type of vibration	Frequency cm^{-1}
PAP	N–H stretch	3364
	Aromatic C–H stretch	3033
	N–H bend	1591
	–N=N–	1414
	C=S	1124
	C–S	827
ND/PAP/MWCNT/PA nanofiber	N–H stretch	3389
	Aromatic C–H stretch	3010
	Aliphatic C–H stretch	2955
	Amide C=O	1642
	N–H bend	1588
	–N=N–	1415
	C=S	1129
ND/PAP/MWCNT/PA/PBAE 1	O–H stretch	3477
	N–H stretch	3311
	Aromatic C–H stretch	3012
	Aliphatic C–H stretch	2899
	Amide C=O	1632
	N–H bend	1594
	–N=N–	1411
	C–O	1334
	C=S	1122

3. Results and Discussion

3.1. Synthesis of nanofiber and nanocomposites

Poly(bisphenol A-co-epichlorohydrin)-based nanocomposites have been prepared by the electrospinning of two types of nanofiller polyamide-*grafted*-nanotube and nanodiamond with new poly(azo-pyridine). Here, electrospinning acted as a useful technique for the alignment of nanofiller in the matrix during the process without compromising the structural integrity of the individual MWCNT or ND. The structure of nanofiber and nanocomposites produced were investigated using FTIR and the results were found to be in

agreement with the proposed structure. ND/PAP/MWCNT/PA nanofiber displayed stretching and bending secondary amine vibrations at 3389 and 1588 cm^{-1} (Fig. 1 A). Aliphatic and aromatic C–H stretching vibration appeared at 2955 and 3010 cm^{-1}. In addition, –N=N– and C=S groups were found at 1415 and 1123 cm^{-1} respectively. For the ND/PAP/MWCNT/PA/PBAE membrane, secondary amine stretching and bending vibrations were found at 3311 and 1594 cm^{-1} (Fig. 1 B). Here again, azo and thiourea groups appeared at 1411 and 1122 cm^{-1} respectively. In the composite structure, a broad stretching vibration at 3477 cm^{-1} indicated the presence of hydroxyl group of epoxy. The O–H stretching vibration was absent in the case of nanofiber. The ring opening reaction of epoxide with amine caused aliphatic stretching vibration at 2899 cm^{-1}, however aromatic proton also appeared at 3012 cm^{-1}. In ND/PAP/MWCNT/PA/PBAE, the characteristic C–O stretching was observed at 1334 cm^{-1}, this peak was also missing in Fig. 1 A. Nevertheless, the appearance of amide group at 1642 and 1632 cm^{-1}, in ND/PAP/MWCNT/PA and ND/PAP/MWCNT/PA/PBAE respectively, indicated the polyamide chains bonded to the side wall of MWCNT.

3.2. Tensile strength

Tensile tests for ND/PAP/MWCNT/PA/PBAE and PAP/MWCNT/PA/PBAE are shown in Table 2 and Fig. 2. The reinforcement of epoxy with nanofibers increased toughness of the system relative to the brittleness of pristine epoxy. ND/PAP/MWCNT/PA/PBAE 1 with 1 wt. % nanofiber loading had the tensile stress of 330.3 MPa, whereas the maximum stress value was observed for ND/PAP/MWCNT/PA/PBAE 3 as 341.3 MPa. The elongation at break of ND/PAP/MWCNT/PA/PBAE 1 membrane was found to be 29.1 percent, while in the case of ND/PAP/MWCNT/PA/PBAE 3 it increased up to 29.7 percent. In these membranes, the addition of 3 wt. % ND/PAP/MWCNT/PA gave 37.7 GPa tensile modulus, at this point again the tensile modulus was lower for lower loading (1 wt. %) of ND/PAP/MWCNT/PA (34.5 GPa). Toughness of ND/PAP/MWCNT/PA/PBAE 1-3 nanocomposites was also increased by the filler loading from 8771-9025 MPa. On the other hand, the system with out nanodiamond inclusion showed lower values in tensile properties depicting the effect of filler in the electrospun nanofibers. Consequently, the PAP/MWCNT/PA/PBAE 1-3 membranes had lower tensile stress, strain, modulus and other tensile properties relative to ND/PAP/MWCNT/PA/PBAE 1-3 membranes. Addition of 1 to 3 wt. % PAP/MWCNT/PA nanofiber in PBAE resulted in tensile strength of 288.1-299.9 MPa. PAP/MWCNT/PA/PBAE 1 had elongation at break of 21.1 percent that increased slightly to 24.3 percent in PAP/MWCNT/PA/PBAE 3. In PAP/MWCNT/PA/PBAE cast membranes, the addition of 3 wt. % ND/PAP/MWCNT/PA gave tensile modulus of 24.6 GPa, at this juncture also the tensile modulus was lower for 1 wt. % ND/PAP/MWCNT/PA loading as 20.9 MPa. Toughness of this system was also lower 6543-7723 MPa compared with nanodiamond-based system. The steady and combined effect of nanodiamond/nanotube increased the overall strength of polymer/nanotube/nanodiamond fiber, thus increasing the stress transfer of ND/PAP/MWCNT/PA/PBAE nanocomposites. Moreover, the new nanofibrous membranes formed had enhanced mechanical profile relative to analogous reported systems [30, 31].

Table 2 Mechanical properties of ND/PAP/MWCNT/PA and PAP/MWCNT/PA nanofiber reinforced films.

Composition	Ultimate Tensile Stress (MPa)	Elongation at break	Tensile Modulus (GPa)	[1]Toughness (MPa)
PAP	28.0	0.40	0.51	19.7
[2] ND/PAP/MWCNT/PA/PBAE 1	330.3	29.1	34.5	8771
ND/PAP/MWCNT/PA/PBAE 2	335.1	29.5	35.9	8940
ND/PAP/MWCNT/PA/PBAE 3	341.3	29.7	37.7	9025
PAP/MWCNT/PA/PBAE 1	288.1	21.1	20.9	6543
PAP/MWCNT/PA/PBAE 2	291.3	23.4	22.2	6998
PAP/MWCNT/PA/PBAE 3	299.9	24.3	24.6	7723

[1] Toughness was determined by integrating the area under the stress-strain curve.

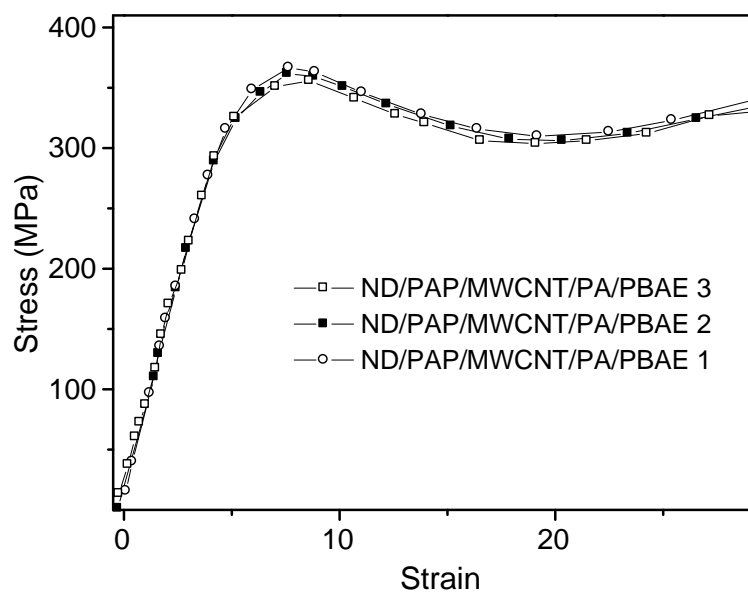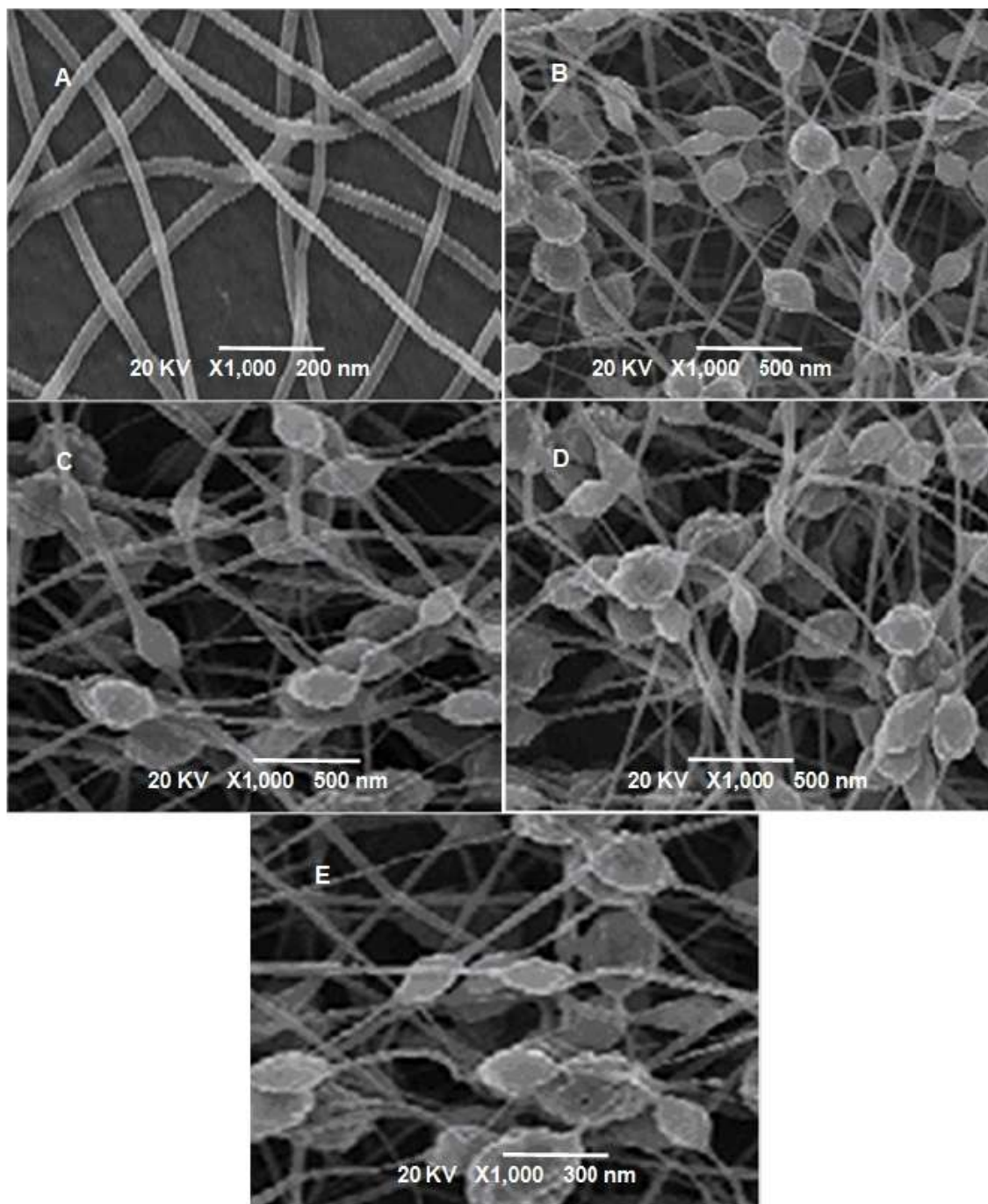[2] The number in the sample designation refers to wt. % of nanofibers in the sample.

Figure 2 Stress-strain curves of ND/PAP/MWCNT/PA/PBAE films.

Figure 3 FESEM images of (A) ND/PAP/MWCNT/PA nanofiber; (B) ND/PAP/MWCNT/PA/PBAE 1;
(C) ND/PAP/MWCNT/PA/PBAE 2; (D) ND/PAP/MWCNT/PA/PBAE 3 (500 nm); (E) ND/PAP/MWCNT/PA/PBAE 3 (300 nm).

3.3. Morphology

SEM image of nanodiamond embedded PAP/MWCNT/PA electrospun nanofiber morphology is presented in Fig. 3A. The modified MWCNT seemed to be orderly oriented along the fiber axis, so resulted in the regular fiber diameter. Consequently, smooth NDPAP/MWCNT/PA fibers were formed during electrospinning process from the polymer/filler solution of appropriate concentration. SEM images of the fracture surfaces of ND/PAP/MWCNT/PA/PBAE 1-3 are presented in Fig. 3 B-E. Optimization of polymer-*grafted*-MWCNT, azopolymer and nanodiamond content was an important step to yield high performance nanofiber. When these nanofibers were employed as reinforcement in epoxy matrix, non-woven nanofibrous web-like morphology was observed. Nanodiamond-based system ND/PAP/MWCNT/PA/PBAE formed beaded fiber like structure, however the nanofiber were evenly coated with the epoxy. On the polymer coated nanofiber, at various places, spherical beads were also formed due to the agglomeration of matrix. The existence of beads within ND/PAP/MWCNT/PA/PBAE scaffold suggested lack of interaction between fibers and epoxy resin at various places. With the increase in nanofiber loading, there was an increased fiber entanglement. Moreover, the size of aggromelated polymer beads increased with in the composite structure (Fig. 3 D & E). Materials presenting such type of unique nanofiber web morphology have been enormously important as nanofiberous filtration media for various contaminants [30]. Here, the control of fiber diameter may improve the contaminant holding capacity of new membranes.
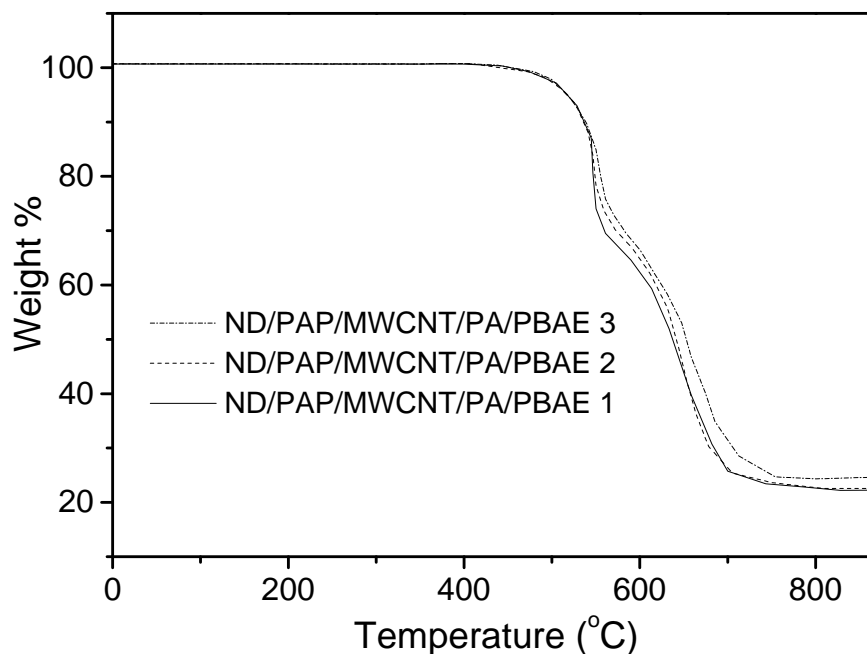
Figure 4 TGA curves of ND/PAP/MWCNT/PA/PBAE 1-3 films at a heating rate 10 ^{o}C/min in N$_2$.

3.4. Thermal properties

Fig. 4 and Table 3 represent TGA results for the nanofibrous membranes. The degradation temperature was well above 500 °C representing good thermal stability. However, the stability of neat PAP was lower with initial degradation temperature T_0 484 °C, 10 % weight loss T_{10} 498 °C, and maximum decomposition T_{max} 588 °C. In the case of PAP/MWCNT/PA/PBAE 1-3 (system with out nanodiamonds) showed lower value in thermal properties. PAP/MWCNT/PA/PBAE 1 had T_0 488 °C, T_{10} 522 °C, and T_{max} 592 °C. With 2 wt. % nanofiber loading, these values increased to T_0 491 °C, T_{10} 528 °C, and T_{max} 599 °C. 3 wt. % PAP/MWCNT/PA nanofiber inclusion further increased the thermal stability as T_0 498 °C, T_{10} 532 °C, and T_{max} 610 °C. On the other hand, nanodiamond-based system ND/PAP/MWCNT/PA/PBAE 1-3 showed improved stability with PAP/MWCNT/PA 1-3 wt. % nanofiber loading as T_0 505-528 °C; T_{10} 536-546 °C; and T_{max} 634-658 °C. Similarly, the char yield of this system was higher 26-29 % relative to PAP/MWCNT/PA/PBAE system 21-24% at 700 °C. The loss tangent (tan δ) of ND/PAP/MWCNT/PA/PBAE 1-3 *vs.* temperature is shown in Fig. 5. The inclusion of nanodiamond-based nanofiber here increased the segmental T_g 301-311 °C as well. Whereas, in the case of PAP/MWCNT/PA/PBAE 1-3 T_g was 244-256 °C. The higher glass transition for the system with nanodiamond pointed to increase in structural rigidity. The synergetic effect of two types of fillers (nanodiamond and carbon nanotube) and two types of polymers i.e. polyamide (chemically linked) and azopolymer (coated) were responsible for the structural rigidity of the nanocomposites. New nanofibrous membranes showed significantly higher thermal stability relative to previous epoxy-based nanocomposites [32, 33].

Table 3 Thermal analyses data of PAP and nanofiber reinforced films.

| Polymer	T_g (°C)	T_0 (°C)	T_{10} (°C)	T_{max} (°C)	Y_c at 700 °C (%)
PAP	210	484	498	588	59
ND/PAP/MWCNT/PA/PBAE 1	301	505	536	634	26
ND/PAP/MWCNT/PA/PBAE 2	303	517	539	641	27
ND/PAP/MWCNT/PA/PBAE 3	311	528	546	658	29
PAP/MWCNT/PA/PBAE 1	244	488	522	592	21
PAP/MWCNT/PA/PBAE 2	249	491	528	599	23
PAP/MWCNT/PA/PBAE 3	256	498	532	610	24

T_g: Glass transition temperature

T_0: Initial decomposition temperature

T_{10}: Temperature for 10 % weight loss

T_{max}: Maximum decomposition temperature

Y_c: Char yield; weight of polymer remained
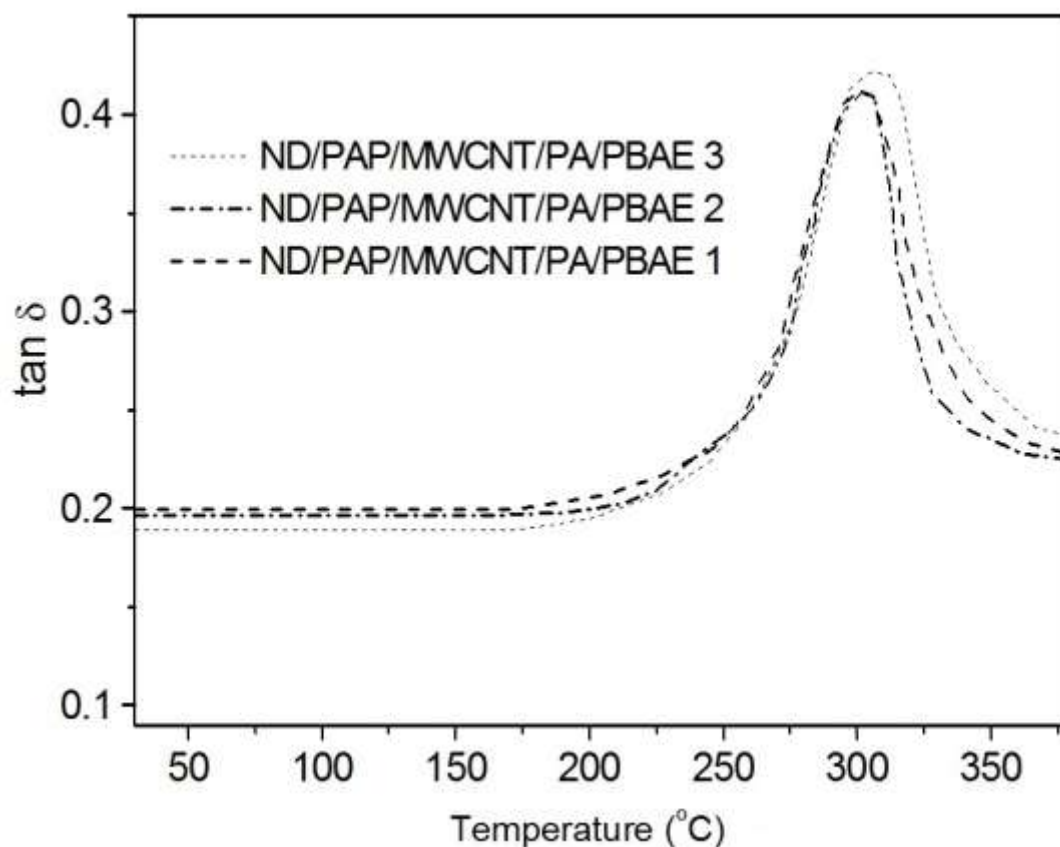
Figure 5 Variation of loss tangent with temperature for ND/PAP/MWCNT/PA/PBAE 1-3.

3.5. Electrical conductivity

ND/PAP/MWCNT/PA/PBAE 1-3 showed considerably higher electrical conductivity values relative to non-nanodimond system (Table 4). The combined effect of nanodiamons, nanotube and azopolymer was found to noticeably enhance the conductivity of the nanocomposites. ND/PAP/MWCNT/PA/PBAE 1 (1 wt. % nanodiamond-based filler) had the conductivity of 4.1 Scm^{-1}, which increased to 5.5 Scm^{-1} for ND/PAP/MWCNT/PA/PBAE 3 (3 wt. % nanodiamond-based filler). Conversely, PAP/MWCNT/PA/PBAE 1 had conductivity of 2.5 Scm^{-1} which was improved to 3.7 Scm^{-1} in PAP/MWCNT/PA/PBAE 3. On the whole, the improvement in the conductivity of ND/PAP/MWCNT/PA/PBAE 1-3 was seemed to be due to the addition of conducting nanodiamond in nanofiber.

Table 4 Conductivity measurement of PAP and nanocomposites.

Sample	Conductivity (S cm^{-1})
PAP	2.2
ND/PAP/MWCNT/PA/PBAE 1	4.1
ND/PAP/MWCNT/PA/PBAE 2	4.9
ND/PAP/MWCNT/PA/PBAE 3	5.5
PAP/MWCNT/PA/PBAE 1	2.5
PAP/MWCNT/PA/PBAE 2	3.2
PAP/MWCNT/PA/PBAE 3	3.7

4. Conclusions

A simple method was employed in this research for the reinforcement of electrospun nanofiber in poly(bisphenol A-co-epichlorohydrin) matrix. Firstly, the polyamide-*grafted*-MWCNT was prepared using *in-situ* polymerization. Two types of nanofibers were then electrospun using azopolymer, modified nanotubes and/or nanodiamond. The PAP/MWCNT/PA and nanodiamond were embedded within structure during electrospinning and well-oriented along the nanofiber axis. Morphological investigation represented the unique web-like nanofiber arrangement with aggromelated polymeric beads dispersed in the nanodiamond-based system. The mechanical and thermal properties of the system were considerably enhanced with the incorporation of small amount of nanodiamond in elecrospun nanofiber. The electrical conductivity of ND/PAP/MWCNT/PA/PBAE nanocomposites reached upto 5.5 Scm^{-1} compared with that of without nanodiamond. Electrical conductivity, macromechanical and thermal properties of both the epoxy systems (PAP/MWCNT/PA/PBAE and ND/PAP/MWCNT/PA/PBAE) were found to increase with nanofiber loading.

5. References

1. Smith Jr JG, Connell JW, Delozier DM, Lillehei PT, Watson KA, Lin Y, Zhou B, Sun Y-P. Space durable polymer/carbon nanotube films for electrostatic charge mitigation. *Polymer.* 2004, 45:825-836

2. Gibson PW, Schreuder-Gibson HL, Pentheny C. Electrospinning technology: direct application of tailorable ultrathin membranes. *J Coated Fabrics.* 1998, 28:63-72

3. Gibson PW, Schreuder-Gibson H, Rivin D. Transport properties of porous membranes based on electrospun nanofibers. *Colloid Surf A: Phys Eng Aspects.* 2001, 187-188:469-481.

4. Wnek G, Carr ME, Simpson D G, Bowlin GL. Electrospinning of nanofiber fibrinogen structures. *Nano Lett.* 2003, 3:213-216

5. Kymakis E and Amaratunga G AJ. Optical properties of polymer-nanotube composites. *Synth Met.* 2004, 142:161-167

6. Haggenmueller R, Gommans HH, Rinzler AG, Fischer JE, Winey KE. Aligned single-wall carbon nanotubes in composites by melt processing methods. *Chem Phys Lett.* 2000, 330:219-225

7. Safadi B, Andrews R, Grulke EA. Multiwalled carbon nanotube polymer composites: synthesis and characterization of thin films. *J Appl Polym Sci.* 2002, 84:2660-2669

8. Jia Z, Wang Z, Xu C, Liang J, Wei B, Wu D, Zhu S. Study on poly(methyl methacrylate)/carbon nanotube composites. *Mater Sci Eng A.* 1999, 271:395-400

9. Andrews R, Jacques D, Minot M, Rantell T. Fabrication of carbon multiwall nanotube/polymer composites by shear mixing. *Macromol Mater Eng.* 2002, 287:395-403.

10. Wu PK, Fitz-Gerald J, Pique A, Chrisey DB, McGill RA. Deposition of nanotubes and nanotube composites using matrix-assisted pulsed laser evaporation. *Mater Res Soc Proc.* 2000, 617:J2.3.

11. Thostenson ET, Li WZ, Wang DZ, Ren ZF, Chou TW. Carbon nanotube/carbon fiber hybrid multiscale composites. *J Appl Phys.* 2002, 91:6034-6037

12. Dersch R, Steinhart M, Boudriot U, Greiner A, Wendorff JH. Nanoprocessing of polymers: applications in medicine, sensors, catalysis, photonics. *Polym Adv Technol.* 2005, 16:276-282

13. Curran SA, Ajayan PA, Blau WJ, Carroll DL, Coleman JN, Dalton AB, Davey AP, Drury A, McCarthy B, Maier S, Strevens A. A composite from poly(m-phenylenevinylene-co-2,5-dioctoxyp-phenylenevinylene) and carbon nanotubes: A novel material for molecular optoelectronics. *Adv Mater.* 1998, 10:1091-1093

14. Norris ID, Shaker MM, Ko FK, MacDiarmid AG. Electrostatic fabrication of ultrafine conducting fibers: polyaniline/polyethylene oxide blends. *Synth Met.* 2000, 114:109-114

15. Bradley K, Gabriel J-C P, Gruner G. Flexible nanotube electronics. *Nano Lett.* 2003, 3:1353-1355

16. Iijima S, Brabec C, Maiti A, Bernholc J. Structural flexibility of carbon nanotubes. *J Chem Phys.* 1996, 104:2089-2092.

17. Lourie O, Cox DM, Wagner HD. Buckling and collapse of embedded carbon nanotubes. *Phys Rev Lett.* 1998, 81:1638-1641.

18. Kim G-M, Michler GH, Potschke P. Deformation processes of ultrahigh porous multiwalled carbon nanotubes/polycarbonate composite fibers prepared by electrospinning. *Polymer.* 2005, 46:7346-7351

19. Bachilo SM, Strano MS, Kittrell C, Hauge RH, Smalley RE, Weisman RB. Structure-assigned optical spectra of single-walled carbon nanotubes. *Science.* 2002, 298:2361-2366

20. Hone J, Llaguno MC, Nemes NM, Johnson AT. Electrical and thermal transport properties of magnetically aligned single wall carbon nanotube films. *Appl Phys Lett.* 2000, **77**:666-6668

21. Breuer O, Sundararaj U. Big returns from small fibers: A review of polymer/carbon nanotube composites. *Polym Comp*. 2004, 25:630-645

22. Yuan X, Zhang Y, Dong C, Sheng J. Morphology of ultrafine polysulfone fibers prepared by electrospinning. *Polym Int.* 2004, 53:1704-1710

23. Zheng YP, Ning RC and Zheng Y. Study of SiO_2 nanoparticles on the improved performance of epoxy and fiber composites. *J Reinfor Plast Comp.* 2005, 24:223-233

24. Reneker D H, Chun I. Nanometre diameter fibres of polymer, produced by electrospinning. *Nanotechnology* 2001, 42:9955-9967

25. Sukhareva LA, Balavintseva EK, Menkova TI, Prostyakov VM. The effect of mesomorphic modifiers on the mechanical and protective properties of epoxy composite systems. *Int J Polym Mater.* 2006, 28:19-22

26. Huang Z M, Zhang Y Z, Kotaki M, Ramakrishna S. A review on polymer nanofibers by electrospinning and their applications in nanocomposites. *Compos Sci Technol.* 2003; 63:2223-2253

27. Kausar A, Hussain ST. Synthesis and properties of poly(thiourea-azo-naphthyl)/multiwalled carbon nanotube composites. *J Plast Film Sheet.* 2013, 30:6-27

28. Deitzel JM, Kosik W, McKnight SH, Ten NCB, Desimone JM, Crette S. Electrospinning of polymer nanofibers with specific surface chemistry. *Polymer*. 2002, 43:1025-1029.

29. Baek J-B, Tan LS. Improved syntheses of poly(oxy-1,3-phenylenecarbonyl-1,4-phenylene) and related poly(ether–ketones) using polyphosphoric acid/P_2O_5 as polymerization medium. *Polymer.* 2003, 44:4135-4147

30. Reneker DH, Chun I. Nanometre diameter fibres of polymer, produced by electrospinning. *Nanotechnology*. 1996, **7**:216-233

31. Chen XH, Chen CS, Chen Q, Cheng FQ, Zhang G, Chen ZZ. Non-destructive purification of multi-walled carbon nanotubes produced by catalyzed CVD. *Mater Lett.* 2002, 57:734-738

32. Demczyk B G, Wang YM, Cumings J, Hetman M, Han W, Zett A, Ritchie RO. Direct mechanical measurement of the tensile strength and elastic modulus of multiwalled carbon nanotubes. *Mater Sci Eng A.* 2002, 334:173-178

33. Kausar A, Hussain ST. Effect of multi-walled carbon nanotubes reinforcement on the physical properties of poly(thiourea-azo-ether)-based nanocomposites. *J Plast Film Sheet.* 2013, 29:365-383